

## Article

# Enhanced Pickering Emulsion Stabilization of Cellulose Nanocrystals and Application for Reinforced and Hydrophobic Coatings

Fan Zhang <sup>1,2,3,\*</sup> , Haoran Tao <sup>1,3</sup>, Yilin Li <sup>1,3</sup>, Yanbing Wang <sup>1,3</sup>, Yingying Zhou <sup>3,4</sup>, Qunna Xu <sup>4</sup> and Jianzhong Ma <sup>2,4</sup>

<sup>1</sup> School of Textile Science and Engineering, Xi'an Polytechnic University, Xi'an 710048, China

<sup>2</sup> Shaanxi Collaborative Innovation Centre of Industrial Auxiliary Chemistry & Technology, Shaanxi University of Science & Technology, Xi'an 710021, China

<sup>3</sup> Key Laboratory of Functional Textile Material and Product (Xi'an Polytechnic University), Ministry of Education, Xi'an 710048, China

<sup>4</sup> College of Bioresources Chemical and Materials Engineering, Shaanxi University of Science and Technology, Xi'an 710021, China

\* Correspondence: zhangfan@xpu.edu.cn

**Abstract:** For oil-in-water (O/W) Pickering emulsions, a new polymer stabilizer of butyl acrylate (BA) grafted cellulose nanocrystals (BA-g-CNC<sub>S</sub>) has been developed. By adjusting the BA concentration, the hydrophilic and hydrophobic surfaces of BA-g-CNC<sub>S</sub> could be systematically modified based on the controllable interface activity. Specifically, the emulsification stability of the as-prepared stabilizer was examined as a function of BA content, BA-g-CNC<sub>S</sub> usage, and oil type. The results showed that the Pickering emulsion stabilized by BA-g-CNC<sub>S</sub> had a 98% volume fraction of emulsion with long-term stability. Importantly, BA-g-CNC<sub>S</sub> could be a promising choice for polymer stabilizers and could generate high internal phase Pickering emulsions without cross-linking when combined with 13% BA and 1.75% BA-g-CNC<sub>S</sub>. Furthermore, it was established that BA-g-CNC<sub>S</sub> possessed self-emulsifying quality, worked as hydrophobic coatings, and improved the mechanical properties. This was of fundamental interest to polymer stabilizer and functional coatings, allowing for promising applications in coating fields such as fabrics, leather, paper, controlled encapsulation, and the release of actives in material science.

**Keywords:** cellulose nanocrystals; stabilizer; Pickering emulsion; coatings; cotton fabric



**Citation:** Zhang, F.; Tao, H.; Li, Y.; Wang, Y.; Zhou, Y.; Xu, Q.; Ma, J. Enhanced Pickering Emulsion Stabilization of Cellulose Nanocrystals and Application for Reinforced and Hydrophobic Coatings. *Coatings* **2022**, *12*, 1594. <https://doi.org/10.3390/coatings12101594>

Academic Editor: Csaba Balázs

Received: 29 September 2022

Accepted: 19 October 2022

Published: 20 October 2022

**Publisher's Note:** MDPI stays neutral with regard to jurisdictional claims in published maps and institutional affiliations.



**Copyright:** © 2022 by the authors. Licensee MDPI, Basel, Switzerland. This article is an open access article distributed under the terms and conditions of the Creative Commons Attribution (CC BY) license (<https://creativecommons.org/licenses/by/4.0/>).

## 1. Introduction

Pickering emulsions have aroused a great deal of excitement in pharmaceuticals, food, agrochemical, paints, cosmetics, and the crude oil recovery field due to “surfactant-free” characteristics [1–3]. It could be further used as template for fabricating porous functional materials [4]. Given that the urgent voices of green chemistry principles, the stabilizer of Pickering emulsions is experiencing a paradigm, converting from solid particles to colloidal particles. Currently, natural colloidal materials such as whey protein [5], soy glycinin [6], kafirin [7,8], zein [9], starch [10], chitosan [11,12], lactic acid [13], casein [14,15], and cellulose [16,17] could satisfy the present demand for eco-friendly stabilizers due to their renewability, nontoxicity, and amphiphaticity. Rod-like cellulose nanocrystals (CNCs) exhibit good mechanical property, oxidation resistance, dispersion stability in water, and biocompatibility, and have become a new research hotspot as a Pickering emulsion stabilizer in recent years [18].

Due to the surface heterogeneity generated by their crystal structure, CNCs are amphiphilic. However, there are several hydroxyl groups on the surface of CNCs, resulting in difficult dispersion in hydrophobic solvents and polymer media [19]. The hydrophilic

of cellulose tends to collect moisture from the environment, lowering the material's mechanical strength [20]. Consequently, it is sometimes required to adjust CNCs in order to improve its hydrophilicity/hydrophobicity, compatibility, and reactivity in practical applications [21]. In order to realize the above characteristics, various kinds of surface modification methods have been applied to CNCs including esterification, etherification, oxidation, silylation, and polymer graft polymerization [22–26]. Among them, polymer graft polymerization is an effective way to overcome the hydrophilicity and compatibility problems, and is used to fabricate functionalized polymer modified nanocellulose composites [27–29]. Recently, most research has focused on polymer grafting nanocellulose composites [30,31], but there have been limited reports on the whole vinyl group modified nanocellulose as a stabilizer. Jianhua Zhou et al. [32,33] carried out reversible addition-fragmentation chain transfer polymerization (RAFT) for the CNC-based block copolymer, which was the sole Pickering stabilizer for Pickering emulsion polymerization. Stephanie A. Kedzior et al. [34] used methyl methacrylate (MMA) to modify nanocellulose by in situ polymerization using polyvinyl alcohol (PVA) as a stabilizing agent. However, the preparation process of block copolymers is time-consuming and has low yields. Taking into account further preventing the crystalline structure of CNCs from being damaged, great efforts have gone into developing modified CNCs. Prior to this,  $\gamma$ -methacryloxypropyl trimethoxysilane (A174) was used for CNC modification to prepare Pickering stabilizers in our previous research. However, this stabilizer displayed inadequate long-term stability, and the prepared CNC-based emulsion had poor film-forming flexibility by Pickering emulsion polymerization.

Herein, BA-g-CNCs were achieved in situ graft polymerization by the ester exchange reaction of surface hydroxyl groups between CNCs and BA, thereby resulting in enhanced compatibility, dispersibility, and wetting properties. We studied parameters such as the BA content, BA-g-CNC concentration, and oil type on the stability of Pickering emulsions. Emulsion stability is described in terms of optical microscopy and tracking the volume fraction of emulsions. The hydrophobic radical carbon-carbon double bond is crucial for stabilizing the O/W interface of the Pickering emulsion and preparing hydrophobic coating materials with improved mechanical performance. This study can provide more ideas and some perspectives on developing CNC-based porous functional material applications in the coatings field for future studies, which is of high theoretical and practical value.

## 2. Materials and Methods

### 2.1. Materials

Cellulose nanocrystals (CNCs) were purchased from the University of Maine (USA). Dichloromethane, paraffin oil, and n-butyl acrylate (BA) was supplied by Tianjin Kemio Chemical Reagents Co. Ltd. (Tianjin, China). N,N-Dimethylacetamide (DMAc, 99.5%), toluene, and cyclohexane were provided by Tianjin Fuyu Chemical Co. Ltd. (Tianjin, China). Tetrabutylammonium acetate (TBAA<sub>C</sub>, 98%) was obtained from Shanghai Macklin Biochemical Co. Ltd. (Shanghai, China). Vegetable oil extracted from soybeans was purchased at the supermarket. All chemicals were of analytical grade and used as received without further purification. Deionized (DI) water through a water purification system was used for the preparation of all aqueous solutions.

### 2.2. Synthesis of Modified Cellulose Nanocrystals

Cellulose nanocrystals (2.5 wt%, 0.2 g) and TBAA<sub>C</sub> (1 g) were immersed in a 50 mL two-necked flask filled in 10 mL DMAc and stirred at 60 °C for 30 min. Subsequently, BA in different mass ratios was simultaneously injected to the system within 30 min. After 2 h, BA-g-CNC<sub>S</sub> were formed and washed several times with DMAc centrifugation. Then, the modified cellulose nanocrystals (BA-g-CNCs) were dispersed in DI water by solvent replacement. The obtained BA-g-CNCs was freeze-dried and present a white powder (Figure S1) for structure characterization and further application.

### 2.3. BA-g-CNC<sub>5</sub> Stabilized for O/W Pickering Emulsions

The O/W type was confirmed by adding a droplet of the Pickering emulsion to the water or oil phase by observing the diffusion. This system changed the BA-g-CNC dosage and oil proportion in the aqueous phase to control the interface activity. To achieve this goal, in a glass vial, BA-g-CNCs were dissolved into 1% (*w/v*) by DI water under a ultrasonic cell pulverizer for 2 min at 30 W. Then, the colorless and transparent BA-g-CNC solutions, as shown in Figure S2, were added dropwise to the oil phase at 0.5 oil fractions. After each step, the mixture was shaken for 10 s. Finally, an IKA T18 homogenizer (IKA (Guangzhou) Instrument and Equipment Co., Ltd, Guangzhou, China) was used to prepare the emulsions at 10,000 rpm for 3 min at 30 °C. The final mixtures were homogenized on a BME100LX high-shear homogenizer equipped for 3 min at 1500 rpm at 20 °C.

### 2.4. Fabrication of Reinforcing and Hydrophobic Cotton Fabric

The cotton fabrics (20 cm × 20 cm) were soaked in water at 70 °C. Then, A174 was added for pretreatment. After the treatment, the treated cotton fabrics were padded with two dips and nips (70%–80% wet pick up) in BA-g-CNC emulsions of 10 g/L. Finally, the cotton fabrics were dried at 80 °C for 3 min and cured at 160 °C for 3 min.

### 2.5. Characterization

Before characterization, the samples were diluted into 0.01 wt% using deionized water. Dynamic light scattering (DLS) was conducted on a Malvern Zetasizer Nano-ZS90 instrument (Malvern Instruments, Worcestershire, U.K.) with 90° backscattering measurements at 25 °C to measure the average particle size. The data were the average of triplicates with 11 to 15 runs for each measurement.

For another test, the samples had to be purified by five centrifugation-dispersion cycles using absolute ethyl alcohol. After drying up, the samples were ground into powder and dried in an infrared-ray oven until their weight reached constantly. Then, KBr was mixed with the same dose of the as-produced powders and pressed in a disk-shaped probing sample for FTIR measurements. The chemical structure of the samples was then determined by a Spotlight 400 FTIR spectrometer (PerkinElmer, Waltham, MA, USA) in the spectra range from 4000 cm<sup>-1</sup> to 400 cm<sup>-1</sup> with a resolution of 4 cm<sup>-1</sup> and a forward and reverse moving mirror speed of 10 and 6.2 kHz, respectively. Thermogravimetric analysis (TGA) and differential thermal gravity (DTG) measurements were carried out by a thermogravimetric analyzer (METTLER TOLEDO TGA/SDTA 851e, Mettoltoldo Technology (China) Co., Ltd, Shanghai, China) with a heating rate of 10 °C/min from 30 to 800 °C in a nitrogen atmosphere. For XRD measurements, a Japan MiniFlex600 X-ray diffractometer (Rigaku Beijing Corporation, Beijing, China) with Cu-Kα radiation ( $k = 0.154$  nm) was utilized for sample crystallinity.

Once Pickering emulsions were generated, the emulsion type was immediately determined by dilution with oil and water: if the emulsion could be dispersed easily in the water phase, it was categorized as O/W type, and if it could be dispersed easily in the oil phase, it was categorized as W/O type. In the meantime, the freshly created emulsion solution was transferred immediately to a 10 mL colorimetric cylinder. The stability of the emulsions and the rate of dehydration were then assessed by measuring the volume fraction of the emulsions after storage at room temperature for varying amounts of time. The creaming/sedimentation index was computed using the formula shown below:

$$\text{The creaming/sedimentation index} = (H_s/H_t) \times 100$$

where  $H_s$  is the height of the serum phase, and  $H_t$  is the total height of the formulation.

Optical microscopy was also visualized using the DM2500M digital biological microscope (Leica, Wetzlar, Germany). A drop of the fresh Pickering emulsion (50% *v/v*) sample was dripped onto the glass slice with a covering slide and then placed on a microscope slide imaged at 50 or 100× magnification.

As a coating material, the as-prepared modified cellulose nanocrystals were applied to cotton fabrics, and their application features such as mechanical and surface hydrophobicity after finishing were evaluated. Before analyzing the qualities of a film, it must be conditioned for 24 h under typical atmospheric conditions. Mechanical properties were evaluated on an AI-3000 universal tensile testing machine (Gotech Testing Machines Inc., Taiwan, China). For each sample (30 cm × 5 cm), the test was carried out three times, from which the average result was calculated.

In addition, the morphology of cotton fabrics was investigated using the SEM equipment KYKY-2800B (KYKY, Beijing, China). Prior to scanning at an acceleration voltage of 5 kV, the samples were gold-sputter-coated to improve their surface conductivity. Contact angle measurements of the untreated and treated cotton fabrics were carried out using a SDC-100 contact angle goniometer (SinDin Precision Instruments Co. Ltd., Dongguan, China) equipped with a dedicated CCD digital camera. A drop of distilled water (3 µL) was placed on the fabric surface at a rate of 0.5 µL/s using a microsyringe at room temperature. Images of the drop were recorded up to 10 s after the drop was set on the fabric surface initially and three locations were tested, from which the average contact angle was determined.

### 3. Results and Discussion

#### 3.1. The Formation Mechanism of BA-g-CNCs

Because of its reactive polar molecule, unsaturated double bond, and carboxylic acid structure, butyl acrylate is utilized to modify or graft the substrate and the obtained copolymers or homopolymers could achieve superior weather, UV, water, and heat resistance [35–37]. This study chose BA to modify CNCs using in situ graft polymerization. The reaction structures of the BA-g-CNCs is shown in Figure 1a. By modifying CNCs, their hydrophilicity could be lowered. The BA-g-CNCs, on one hand, possess both hydrophilicity and hydrophobicity and can be employed to stabilize the Pickering emulsion (Figure 1b). The interfacial stabilization of BA-g-CNCs may be used to build unique structures or functional polymer composites via the Pickering emulsion polymerization technology. On the other hand, BA-g-CNCs have excellent adhesion to hydrophobic substrates and increased chemical compatibility with hydrophobic substrates. The interfacial action of BA-g-CNCs for targeted functional cellulose coatings are presented in Figure 1c.

As depicted in Figure S3, the unmodified CNCs are highly agglomerated and have an uneven particle size distribution due to their high hydrophilicity. In the TBAA<sub>C</sub>/DMAc solvent system, the ester exchange reaction was conducted between BA and the surface hydroxyl groups of CNCs, resulting in the production of BA-g-CNCs with a narrow distribution and a particle size of 70 nm. The prepared BA-g-CNCs had hydrophobic double bond groups. By varying the BA dosage, the hydrophobicity of BA-g-CNCs and coverage in the Pickering emulsion droplet may be controlled, which plays a crucial role in boosting the interfacial stability of the Pickering emulsion and the performance of the target coatings.

As shown in Figure 1b, when BA-g-CNCs were used as the Pickering stabilizer, the obtained BA-g-CNCs were able to adsorb well at the oil/water interface, relying on van der Waals and hydrogen bonding, forming an interfacial film with a large coverage area and reducing the interfacial tension. Thus, the Pickering emulsion stabilized by BA-g-CNCs had improved stability and a smaller average droplet size. When the BA-g-CNCs were employed as enhanced mechanical property and hydrophobic coating materials, they were dipped–rolled–dipped into A174-treated cotton fabric (Figure 1c). The treated cotton fabric containing silicon hydroxyl groups can be condensed with adjacent silicon hydroxyl groups while condensing the hydroxyl groups on BA-g-CNCs, resulting in anchoring BA-g-CNCs to the surface of the cotton fabric by chemical bonds. Thus, modified CNCs acted as reinforcing agents for transferring interfacial stress via the chemical interactions between them and the substrates, imparting the substrates with exceptional mechanical performance. Moreover, due to double bond groups and a rough surface, the BA-g-CNCs coatings endowed the cotton fabric with hydrophobicity.

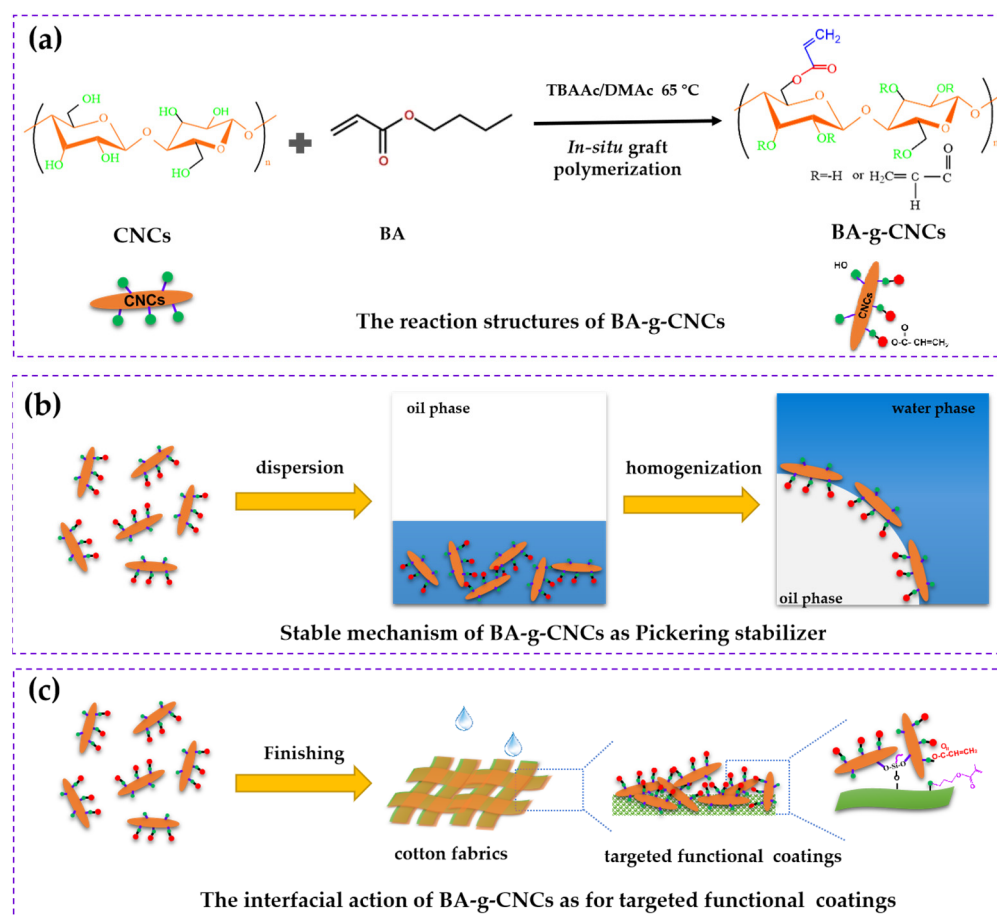


**Figure 1.** (a) The reaction structures of BA-g-CNCs, (b) the stable mechanism as a Pickering stabilizer, and (c) the interfacial action for targeted functional coatings.

### 3.2. The Structures of BA-g-CNCs

To elucidate the successful synthesis of BA-g-CNCs, their structures were examined using FTIR, XRD, and TGA-DTG. As demonstrated in Figure 2a, the FTIR spectra of CNCs and synthesized BA-g-CNCs exhibited chemically distinctive vibrations, respectively. The typical characteristic bands of CNCs at around  $3336\text{ cm}^{-1}$ ,  $2902\text{ cm}^{-1}$ ,  $1369\text{ cm}^{-1}$ , and  $1041\text{ cm}^{-1}$  were associated with the  $\text{-OH}$  stretching,  $\text{C-}\geq\text{H}$  stretching,  $\text{C-H}$  bending vibration, and  $\text{C-O}$  stretching, which is consistent with previously published studies [38]. Comparing the FTIR spectra of CNCs, the spectra of the BA-g-CNCs obviously possessed additional vibrations at  $1609\text{ cm}^{-1}$ , which were assigned to the stretching vibration of  $\text{C=C}$  on BA. These distinctive peaks suggest that BA had been successfully grafted onto CNCs. In addition, the crystallite structure of the CNCs and produced BA-g-CNCs was analyzed using XRD analysis and is displayed in Figure 3b. It can be seen that CNCs and the synthesized BA-g-CNCs had characteristic diffraction peaks at  $15.4^\circ$ ,  $16.5^\circ$ , and  $22.9^\circ$ , corresponding to the diffraction absorption peaks of the 101-crystal plane,  $10\bar{1}$ -crystal plane and 002 crystal planes, respectively. It was indicated that CNCs belong to the typical cellulose I pattern regardless of the modification. The peak intensities of BA-g-CNCs were higher than those of CNCs. These distinctive peaks demonstrated that the hydrophobic alteration of CNCs by BA will not alter their crystal structure. TGA and DTG provided further help for the effective preparation of BA-g-CNCs [39]. As demonstrated in Figure 2c,d, as the temperature rose from 25 to  $800\text{ }^\circ\text{C}$ , the CNCs and BA-g-CNCs exhibited different weight loss and weight loss rates. The thermal degradation process of CNCs resulted in approximately 6.4% mass loss at temperatures below  $150\text{ }^\circ\text{C}$ , followed by 50.6% mass loss between  $297\text{ }^\circ\text{C}$  and  $400\text{ }^\circ\text{C}$ . During this process, the majority of the CNC

structure was thermally damaged, with the greatest disintegration rate occurring at 308 °C. In the literature, similar heat degradation tendencies have also been described [40]. In contrast to the TGA–DTG curves of CNCs, the thermal degradation of BA-g-CNCs occurred in three stages. The initial step was water evaporation prior to 120 °C. Subsequently, the BA-g-CNCs decomposed in the range of 125–275 °C, primarily due to the thermal degradation of the grafted butyl acrylate segment. In the third stage, the weight loss was approximately 28.9% in the range of 275–400 °C, and the greatest weight loss rate occurred around 319 °C, catalyzed by CNCs in BA-g-CNCs. It is intriguing that the initial thermal disintegration of CNCs began at 295 °C, while BA-g-CNCs began at 125 °C. The lower breakdown temperature of BA-g-CNCs may have been caused by the lower glass transition temperature of the acrylates grafted onto the surface of the CNCs via transesterification, hence lowering the thermal stability of the BA-g-CNCs.

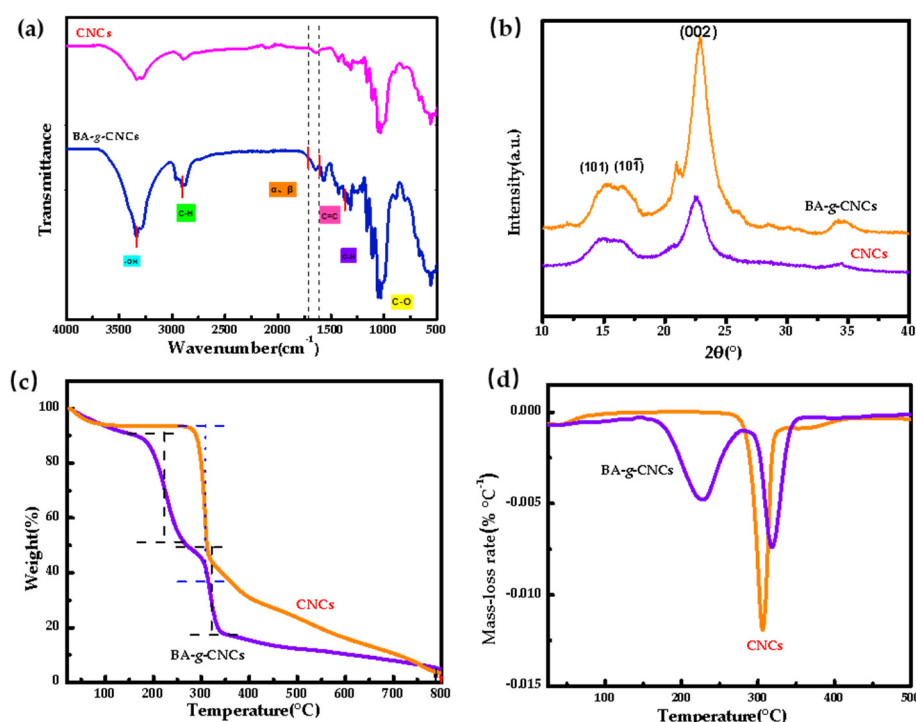


**Figure 2.** (a) FTIR spectra, (b) X-ray diffraction patterns, (c) TGA, and (d) DTG curves of CNCs and BA-g-CNCs.

### 3.3. Stability and Morphology of O/W Pickering Emulsions of BA-g-CNCs as Pickering Stabilizers

The nature of colloidal particles determines the type and stability of a Pickering emulsion [18,41]. This study primarily studied the impact of the modifier, O/W ratio, and stabilizer concentration on the Pickering emulsion stability. According to the emulsion height variation and optical microscope images, the degree of alteration of CNCs and the stabilization impact of BA-g-CNCs were determined (see Figures 3–5) [42]. Figure 3 depicts the optical microscope images, the corresponding emulsion appearance after standing for 24 h, and the volume fraction of the Pickering emulsion stabilized by BA-g-CNCs with various BA concentrations. The optical microscope images indicated that butyl acrylate was successful in altering the hydrophilicity and hydrophobicity of the CNC surfaces and that the generated BA-g-CNCs had a good stabilizing effect. When the BA concentration was less than 13%, the emulsion droplet was less homogenous and contained small oil phase droplets that had not been emulsified. This is due to the fact that when the BA content of the modifier is low, the surface of the BA-g-CNCs contains more –OH, the hydrophilicity is still stronger, and the adsorption energy barrier is higher [43], so it cannot completely form an interfacial film covering a large area in the O/W interface, resulting in the formation of small droplets in the oil phase under the action of external forces. When

the BA concentration exceeds 13%, the emulsion droplets will collect across a vast region and be extruded and distorted by one another. This is due to the excessive amount of BA, the strong hydrophobicity of BA-g-CNCs, and the rise in interfacial tension and interfacial adsorption energy, all of which make it challenging to suppress Pickering emulsion droplet aggregation, hence decreasing the emulsion stability. According to the volume fractions of the emulsion after emulsification (Figure 3f), the Pickering displacement stability first increased and then decreased with increasing BA content, which was consistent with the appearance of the emulsion and optical microscope images of the corresponding samples after 24 h of resting.

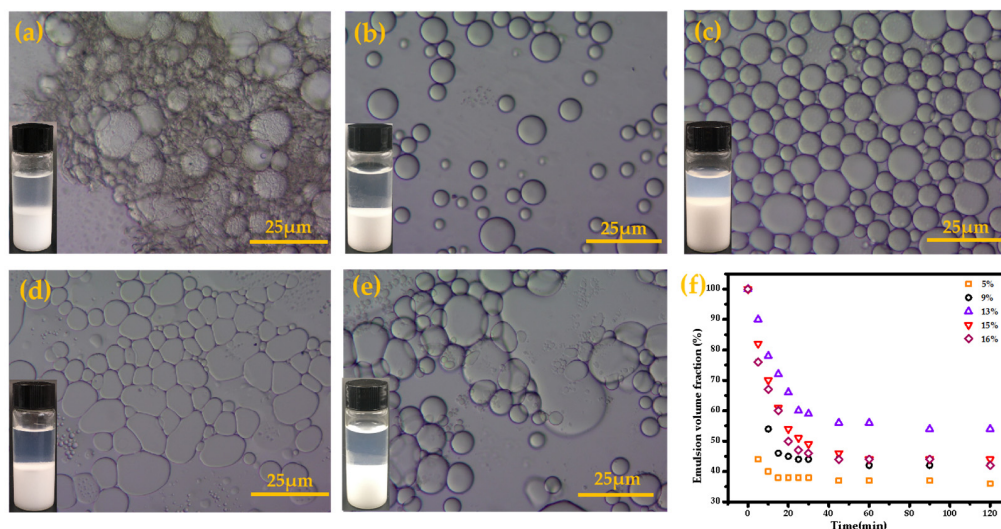


**Figure 3.** (a–e) Optical micrographs and the corresponding height diagrams of the BA-g-CNC stabilized Pickering emulsions after standing for 24 h at different usages of BA: (a) 5%, (b) 9%, (c) 13%, (d) 15%, (e) 16%; (f) their emulsion volume fraction. The sample concentration was fixed at 0.25% ( $w/v$ ). The O/W ratio was 1:1; The oil phase was dichloromethane.

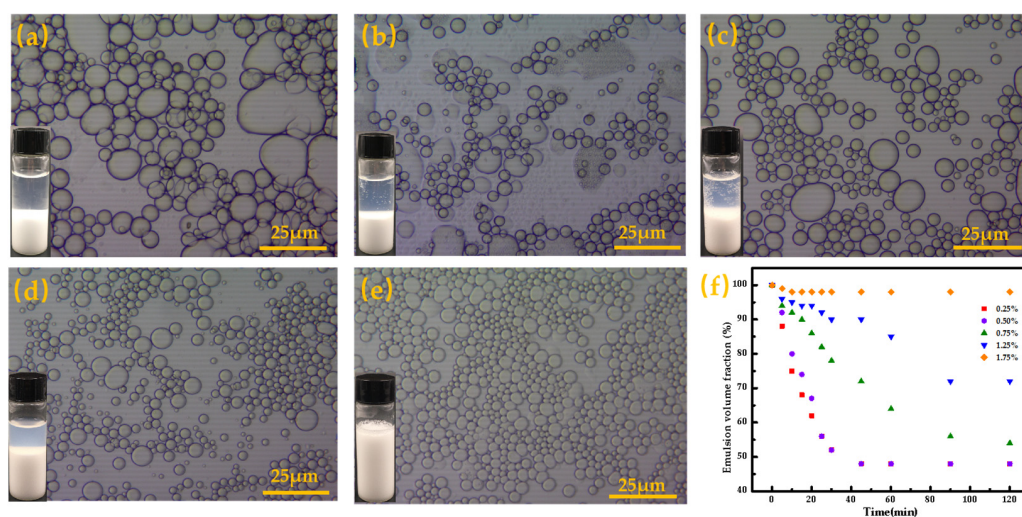


**Figure 4.** Optical micrographs (a–e) and the corresponding height diagram of Pickering emulsions stabilized by BA-g-CNCs after standing for 24 h at different usages of BA-g-CNCs: (a) 0.25%, (b) 0.50%, (c) 0.75%, (d) 1.25%, (e) 1.75%, and (f) their emulsion volume fraction. The O/W ratio was 6:4; The oil phase was dichloromethane.

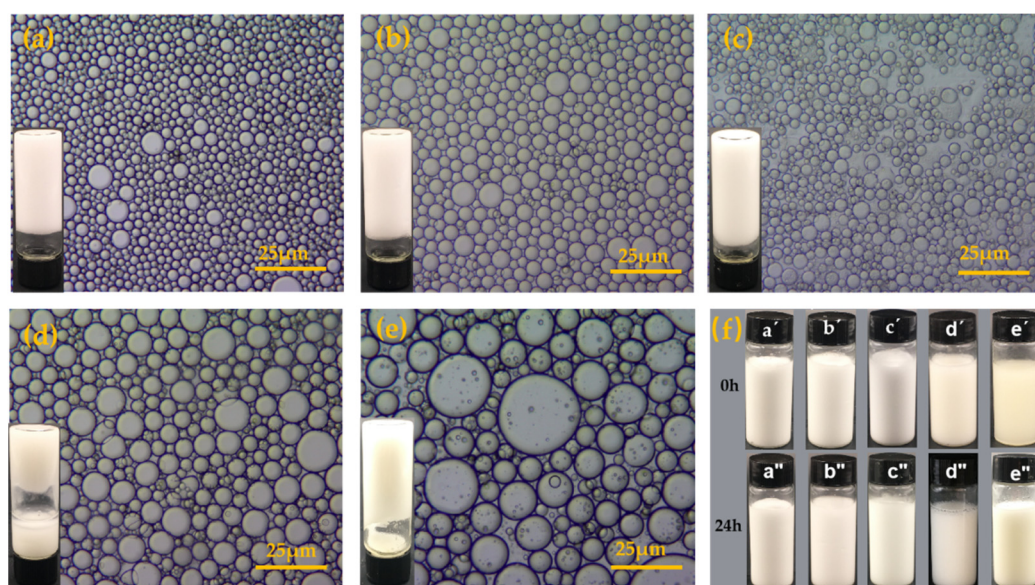


**Figure 5.** Optical microscope images (a–e) and the appearance of the corresponding inverted Pickering emulsions stabilized by BA-g-CNCs in different oil dispersions: (a, a', a'') toluene, (b, b', b'') cyclohexane, (c, c', c'') dichloromethane, (d, d', d'') paraffin oil, (e, e', e'') vegetable oil. (f) Height diagram of stabilized emulsions standing for 0 h (a'–e'), 24 h (a''–e''). The concentration of BA-g-CNCs was fixed at 1.75% (*w/v*). The O/W ratio was 6:4.

Adjusting the number of BA-g-CNCs added in order to examine the effect of the Pickering stabilizer concentration on the stability of Pickering emulsions while keeping all of the other parameters constant. According to Figure 4a–e, when the concentration of BA-g-CNCs was low, the emulsion droplets with a uniform size were compressed and distorted, and oil phase droplets were evident. As the stabilizer concentration of the BA-g-CNCs grew, the volume of emulsion delamination reduced gradually. As depicted in Figure 4e, when the concentration of BA-g-CNCs was 1.75%, the produced emulsion was stable, and droplets were disseminated in a continuous phase as unconnected spheres with uniform distribution. After 24 h of standing, no delamination phenomenon was seen. This suggests that sufficient BA-g-CNCs could thoroughly cover the oil/water interface to prevent oil droplets from aggregating and producing a stable emulsion. Similar conclusions were reached for the volume fractions of emulsions based on their resting stability and optical microscope images. Within two hours, the volume fraction of the emulsion changed significantly before remaining constant. As demonstrated in Figure 4f, as the concentration of BA-g-CNCs increased, so did the volume fraction of the emulsion until no delamination occurred. When the BA-g-CNC concentration was 1.75%, the resulting emulsion was more viscous and gel-like, and it did not move when inverted, generating high internal phase Pickering emulsions. Cross-linker agents were required to provide long-term stability when polymer nanoparticles were utilized as stabilizers to create a high internal phase emulsion [44], as reported. In this study, uncross-linked BA-g-CNCs could generate a very stable Pickering emulsion with a high internal phase, which is anticipated to develop additional porous functional materials for pharmaceutical, aesthetic, and tissue engineering applications [4,45].

This work utilized toluene, cyclohexane, dichloromethane, paraffin oil, and viscous edible vegetable oil to see whether BA-g-CNCs could be universally used with various oil phases to produce stable water-in-oil high internal phase Pickering emulsions. Figure 5a–e displays images taken by an optical microscope of various oil phase emulsions stabilized by BA-g-CNCs. Herein, all emulsions were the O/W type. According to the micromorphology of emulsion droplets, the emulsion droplet size was uniform and dense without voids. The corresponding inverted appearance diagram showed that only the emulsion prepared with

the oil phase of paraffin oil was shifted, which is related to the low viscosity of paraffin oil itself. The high internal phase Pickering emulsion could be prepared with other oil phases. Due to the moderate concentration of BA-g-CNCs being adsorbed at the oil/water interface and the C=C bonds on its surface being organized in the droplet dispersion phase, Pickering emulsions were significantly stabilized. In addition, according to the findings of Tamba's study, the interparticle forces were not negligible when the particle concentration at the interface was high enough [46]. Strong intermolecular interactions between adjacent BA-g-CNCs further stabilized the effect, resulting in a high internal phase emulsion. As depicted in Figure 5f and Figure S4, the emulsion volume fraction never changed after standing for 24 h. This demonstrates that BA-g-CNCs had high emulsification stability for all oil phases.

### 3.4. BA-g-CNCs as Reinforcing and Hydrophobic Cotton Fabric Coatings

CNCs are commonly utilized as a reinforcing filler in composite materials due to their exceptional strength and rigidity [47]. Unlike inorganic nanofillers, it is non-polluting, natural, renewable, and biocompatible. In the meantime, modified CNCs showed increased hydrophobicity, and BA could enhance the film formation and flexibility of the target BA-g-CNC coatings. Herein, the superior BA-g-CNCs are therefore suggested to treat cotton fabrics as reinforced and hydrophobic coatings. The morphology of the BA-g-CNC finished cotton fabrics with varying BA concentrations was observed by SEM. As shown in Figure 6a, the cotton fiber finished with unmodified CNCs contained clusters of nanocellulose whiskers with an uneven distribution. This is due to hydrogen bonding and van der Waals forces absorbing CNCs on the fiber surface. On the other hand, the strong hydrogen bonding between unmodified CNCs could cause the CNCs to aggregate, as shown in the basket box in Figure 6. As the BA concentration grew, the hydrophobicity of BA-g-CNCs increased, which formed a smoother coatings under the action of condensed hydroxyl groups between BA-g-CNCs and the fabrics, resulting in fiber adhesion, illustrated in Figure 6b–d. With the continuous increase in the BA concentration, the hydroxyl group on the surface of BA-g-CNCs diminished. It is difficult to form BA-g-CNC coatings on the cotton fabric surface because of the reduced contact force, as seen in Figure 6e,f, as shown by the red arrows. Therefore, the morphology of BA-g-CNCs on the surface of cotton fabrics significantly impacts the mechanical property and hydrophobicity.

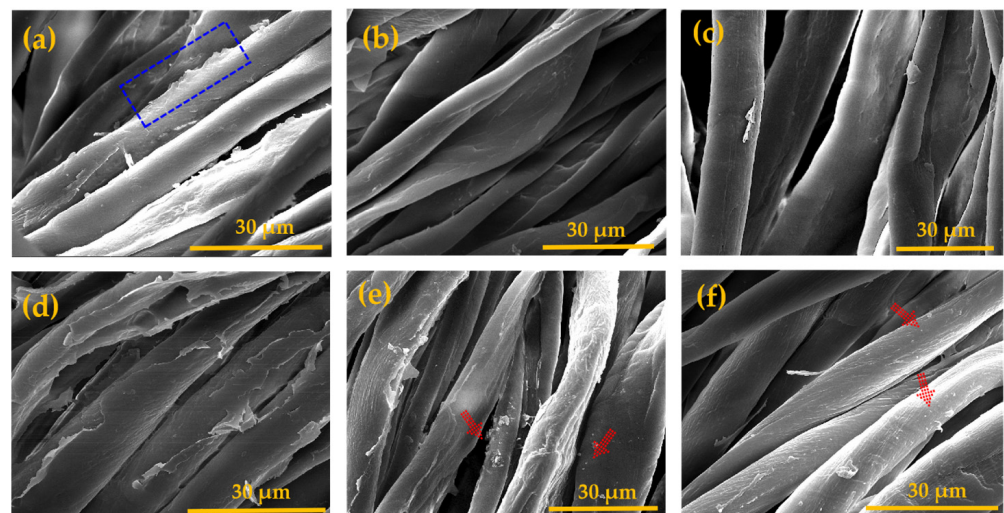


**Figure 6.** SEM of the finished cotton fabrics by BA-g-CNCs under different BA concentrations: (a) 0%, (b) 5%, (c) 9%, (d) 13%, (e) 15%, (f) 16%.

To further understand the above-mentioned reinforcing and hydrophobicity, the contact angle and mechanical properties were investigated. Figure 7 presents the contact angles of cotton fabrics treated with BA-g-CNCs with varying BA concentrations. It can be noted that the unmodified CNC finished cotton fabric was hydrophilic with  $82^\circ$ . As the concentration of BA grew, the contact angle of BA-g-CNC treated cotton fabrics increased from  $87^\circ$  to  $100^\circ$  and then dropped. In other words, the cotton fabrics changed from initially being hydrophilic to hydrophobic. This is because the hydrogen link between the hydroxyl groups of BA-g-CNCs and cotton fabric gradually weakens as the degree of alteration of CNCs rises, causing a morphology change from the coating to aggregate on the cotton fabric surface (see Figure 6). When BA-g-CNCs formed thin films on the cotton fabric surface, the water contact angle increased due to the hydrophobicity of BA-g-CNCs. In contrast, when the BA content was higher than 12%, the BA-g-CNCs were excessively modified with strong hydrophobicity. It was difficult for BA-g-CNCs to finish on a cotton fabric. Only a small amount of BA-g-CNCs aggregated rather than the coatings on the surface of the cotton fabric. Therefore, the water contact angle ( $79^\circ$ ) of the finished cotton fabric at 16% of the BA content was close to that of the original unmodified CNC finished cotton fabric.

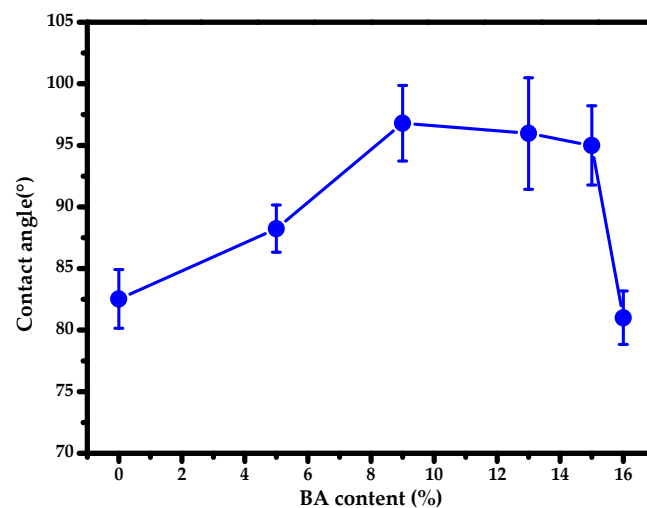


**Figure 7.** Effect of the BA content on the contact angle of the finished cotton fabrics by BA-g-CNCs.

As shown in Figure 8, the mechanical properties of cotton fabrics treated with BA-g-CNCs containing varying amounts of BA were conducted. It was observed that cotton fabrics processed by BA-g-CNCs exhibited superior mechanical properties compared to those processed by unmodified CNCs. Meanwhile, as the BA content increased, the mechanical performance of the fabric samples improved. The breaking tenacity was increased from 4.30 to 5.67 MPa and the elongation at break was discovered to increase from 21% to 24.75%. This is because CNCs have a greater specific surface area and are more rigid, which could impart good mechanical performance to cotton fibers by forming coatings. However, at a 15% BA content, too much BA content resulted in a decrease. In this case, a large number of BA-g-CNC aggregates on the surface of the cotton fabric would result in stress concentration and a decrease in mechanical performance by transferring interfacial stress between them and the substrates. The data at the 16% BA content showed some variation due to the uneven fabric finishing and sampling location, but it had no effect on the overall trend. The results of the contact angle and mechanical properties were consistent with the morphology of the cotton fabric, as depicted in Figure 6.

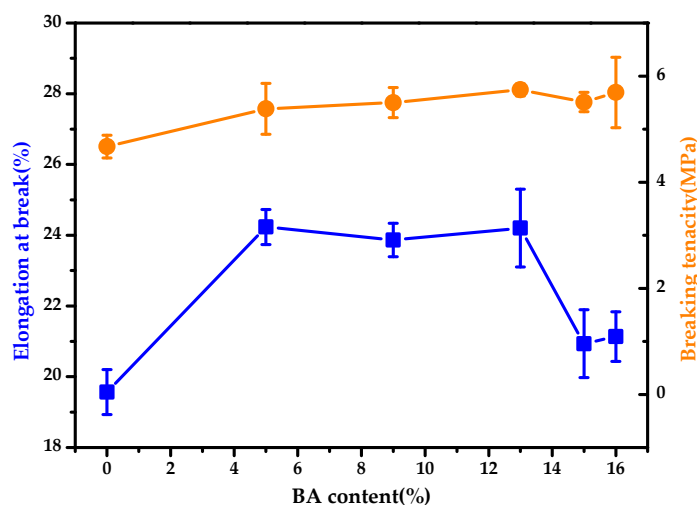


**Figure 8.** Effect of the BA content on the mechanical properties of finished cotton fabrics by BA-g-CNCs.

#### 4. Conclusions

Through in situ graft polymerization of CNCs with BA, BA-g-CNCs were successfully synthesized as Pickering stabilizers and reinforcing/hydrophobic coatings. The use of BA altered the amphiphilicity of BA-g-CNCs. Pickering emulsions stabilized by BA-g-CNCs have an optimized droplet size distribution and excellent stability without layering when the BA content was 13%, the BA-g-CNC dosage was 1.75%, and the O/W ratio was 6:4. The BA-g-CNCs formed a film on the surface of the cotton fabric as a finishing agent, which significantly improved the mechanical and hydrophobic properties. Furthermore, BA-g-CNCs could be used to stabilize different oil phases in order to create high internal phase Pickering emulsions. This study demonstrates a simple method for preparing modified CNCs as stabilizers and reinforcing/hydrophobic coatings as well as a method to design functional porous nanoparticles based on CNCs.

**Supplementary Materials:** The following supporting information can be downloaded at: <https://www.mdpi.com/article/10.3390/coatings12101594/s1>, Figure S1: Physical appearances of BA-g-CNCs powder; Figure S2: Appearance of the front (a) and bottom(b) of 0.4% (w/v) BA-g-CNCs solution with 13% of BA content; Figure S3: DLS of CNCs and BA-g-CNCs; Figure S4: Emulsion volume fraction Pickering emulsions stabilized by BA-g-CNCs in different oil dispersion.

**Author Contributions:** Conceptualization, F.Z.; methodology, H.T.; investigation, Y.L.; data curation, Y.Z.; writing—original draft preparation, F.Z.; writing—review and editing, Q.X. and Y.W.; supervision, J.M.; funding acquisition, F.Z. All authors have read and agreed to the published version of the manuscript.

**Funding:** This work was financially supported by the National Science Foundation of China (21908171), the Shaanxi Provincial National Science Foundation (2020JQ-825, 2021JQ-665), the Shaanxi Provincial Education Fund (21JK0647), and the Open Project of Shaanxi Collaborative Innovation Center of Industrial Auxiliary Chemistry and Technology (No. XTKF-2019-04).

**Institutional Review Board Statement:** Not applicable.

**Informed Consent Statement:** Not applicable.

**Data Availability Statement:** The data presented in this study are available on request from the corresponding author.

**Acknowledgments:** The authors would like to thank all of the reviewers who participated in the review.

**Conflicts of Interest:** The authors declare no conflict of interest.

## References

1. Perrin, L.; Gillet, G.; Gressin, L.; Desobry, S. Interest of Pickering emulsions for sustainable micro/nanocellulose in food and cosmetic applications. *Polymers* **2020**, *12*, 2385. [[CrossRef](#)]
2. Pirozzi, A.; Ferrari, G.; Donsì, F. The use of nanocellulose in edible coatings for the preservation of perishable fruits and vegetables. *Coatings* **2021**, *11*, 990. [[CrossRef](#)]
3. Parajuli, S.; Alazzam, O.; Wang, M.; Mota, L.C.; Adhikari, S.; Wicks, D.; Ureña-Benavides, E. Surface properties of cellulose nanocrystal stabilized crude oil emulsions and their effect on petroleum biodegradation. *Colloids Surf. A* **2020**, *596*, 124705. [[CrossRef](#)]
4. Had, B.; Cfa, B.; Mad, C.; VS, A.; VH, B. Polymerization of cellulose nanocrystals-based Pickering HIPE towards green porous materials-Science Direct. *Carbohydr. Polym.* **2020**, *243*, 116411.
5. Yi, J.; Gao, L.; Zhong, G.; Fan, Y. Fabrication of high internal phase Pickering emulsions with calcium-crosslinked whey protein nanoparticles for  $\beta$ -carotene stabilization and delivery. *Food Funct.* **2020**, *11*, 768–778. [[CrossRef](#)]
6. Liu, F.; Tang, C.H. Soy protein nanoparticle aggregates as pickering stabilizers for oil-in-water emulsions. *J. Agric. Food Chem.* **2013**, *61*, 8888–8898. [[CrossRef](#)]
7. Liu, F.; Tang, C.H. Soy glycinin as food-grade Pickering stabilizers: PART. I. structural characteristics, emulsifying properties and adsorption/arrangement at interface. *Food Hydrocoll.* **2016**, *60*, 606–619. [[CrossRef](#)]
8. Liu, F.; Tang, C.H. Soy glycinin as food-grade Pickering stabilizers: PART. II. Improvement of emulsification and interfacial adsorption by electrostatic screening. *Food Hydrocoll.* **2016**, *60*, 620–630. [[CrossRef](#)]
9. Ma, J.J.; Huang, X.N.; Yin, S.W. Bioavailability of quercetin in zein-based colloidal particles-stabilized Pickering emulsions investigated by the in vitro digestion coupled with Caco-2 cell monolayer model. *Food Chem.* **2021**, *360*, 130152. [[CrossRef](#)]
10. Pei, X.; Zhai, K.; Wang, C.; Deng, Y.; Wang, P. Polymer brush graft-modified starch-based nanoparticles as Pickering emulsifiers. *Langmuir* **2019**, *35*, 7222–7230. [[CrossRef](#)]
11. Wang, X.Y.; Heuzey, M.C. Chitosan-based conventional and Pickering emulsions with long term stability. *Langmuir* **2016**, *32*, 929–936. [[CrossRef](#)]
12. Mwangi, W.W.; Ho, K.W.; Tey, B.T.; Chan, E.S. Effects of environmental factors on the physical stability of Pickering emulsions stabilized by chitosan particles. *Food Hydrocoll.* **2016**, *60*, 543–550. [[CrossRef](#)]
13. Qi, F.; Wu, J.; Sun, G.; Nan, F.F.; Ngai, T.; Ma, G.H. Systematic studies of Pickering emulsions stabilized by uniform-sized PLGA particles: Preparation and stabilization mechanism. *J. Mater. Chem. B* **2014**, *2*, 7605–7611. [[CrossRef](#)]
14. Guo, Y.; Wu, C.; Du, M.; Lin, S.; Xu, X.; Yu, P. In-situ dispersion of casein to form nanoparticles for Pickering high internal phase emulsions. *LWT* **2021**, *139*, 110538. [[CrossRef](#)]
15. Xu, Q.N.; Ma, J.Z.; Zhou, J.H.; Wang, Y.Y.; Zhang, J. Bio-based core-shell casein-based silica nano-composite latex by double-in situ polymerization: Synthesis, characterization and mechanism. *Chem. Eng. J.* **2013**, *228*, 281–289. [[CrossRef](#)]
16. Hu, Z.; Marway, H.S.; Kasem, H.; Pelton, R.; Cranston, E.D. Dried and redispersible cellulose nanocrystal Pickering emulsions. *ACS Macro Lett.* **2016**, *5*, 185–189. [[CrossRef](#)]
17. Buffiere, J.; Balogh-Michels, Z.; Borrega, M.; Geiger, T.; Zimmermann, T.; Sixta, H. The chemical-free production of nanocelluloses from microcrystalline cellulose and their use as Pickering emulsion stabilizer. *Carbohydr. Polym.* **2017**, *178*, 48–56. [[CrossRef](#)]
18. Dai, H.; Wu, J.; Zhang, H.; Chen, Y.; Ma, L.; Huang, H.; Huang, Y.; Zhang, Y. Recent advances on cellulose nanocrystals for Pickering emulsions: Development and challenge. *Trends Food Sci. Technol.* **2020**, *102*, 16–29. [[CrossRef](#)]
19. Bertsch, B.; Fischer, P. Adsorption and interfacial structure of nanocelluloses at fluid interfaces. *Adv. Colloid Interface Sci.* **2020**, *276*, 102089. [[CrossRef](#)]
20. Li, J.; Xu, Q.; Jin, L.Q. Research development on hydrophobic modification of cellulose nanofibrils. *Adv. Mater. Res.* **2013**, *785–786*, 440–443. [[CrossRef](#)]
21. Parajuli, S.; Ureña-Benavides, E.E. Fundamental aspects of nanocellulose stabilized Pickering emulsions and foams. *Adv. Colloid Interface Sci.* **2022**, *299*, 102530. [[CrossRef](#)]
22. Eyley, S.; Thielemans, W. Surface modification of cellulose nanocrystals. *Nanoscale* **2014**, *6*, 7764. [[CrossRef](#)]
23. Peng, S.X.; Chang, H.; Kumar, S.; Moon, R.J.; Youngblood, J.P. A comparative guide to controlled hydrophobization of cellulose nanocrystals via surface esterification. *Cellulose* **2016**, *23*, 1825–1846. [[CrossRef](#)]
24. Li, M.C.; Mei, C.; Xu, X.; Lee, S.; Wu, Q. Cationic surface modification of cellulose nanocrystals: Toward tailoring dispersion and interface in carboxymethyl cellulose films. *Polymer* **2016**, *107*, 200–210. [[CrossRef](#)]
25. Khanjanzadeh, H.; Behrooz, R.; Bahramifar, N.; Gindl-Altmutter, W.; Bacher, M.; Edler, M.; Griesser, T. Surface chemical functionalization of cellulose nanocrystals by 3-aminopropyltriethoxysilane. *Int. J. Biol. Macromol.* **2018**, *106*, 1288–1296. [[CrossRef](#)]
26. Li, B.; Xu, W.; Kronlund, D.; Maattanen, A.; Liu, J.; Smatt, J.H.; Xu, C. Cellulose nanocrystals prepared via formic acid hydrolysis followed by TEMPO-mediated oxidation. *Carbohydr. Polym.* **2015**, *133*, 605–612. [[CrossRef](#)]
27. Lin, W.S.; Hu, X.; You, X.; Sun, Y.; Wen, Y.; Yang, W.; Chen, H. Hydrophobic modification of nanocellulose via a two-step silanation method. *Polymers* **2018**, *10*, 1035. [[CrossRef](#)]
28. Gan, L.; Liao, J.; Lin, N.; Hu, C.; Wang, H.; Huang, J. Focus on gradientwise control of the surface acetylation of cellulose nanocrystals to optimize mechanical reinforcement for hydrophobic polyester-based nanocomposites. *ACS Omega* **2017**, *2*, 4725–4736. [[CrossRef](#)]

29. Peng, S.X.; Shrestha, S.; Yoo, Y.; Youngblood, J.P. Enhanced dispersion and properties of a two-component epoxy nanocomposite using surface modified cellulose nanocrystals. *Polymer* **2017**, *112*, 359–368. [[CrossRef](#)]
30. Wu, J.; Lu, Q.; Wang, H.; Lu, B.; Huang, B. Controllable construction of temperature sensitive supramolecular hydrogel based on cellulose and cyclodextrin. *Polymers* **2022**, *14*, 3801. [[CrossRef](#)]
31. Dong, W.K.; Shin, J.; Choi, S.Q. Nano-dispersed cellulose nanofibrils-PMMA composite from Pickering emulsion with tunable interfacial tensions. *Carbohydr. Polym.* **2020**, *247*, 116762.
32. Yao, H.; Zhou, J.; Li, H.; Zhao, J. Nanocrystalline cellulose/fluorinated polyacrylate latex via RAFT mediated surfactant-free emulsion polymerization and its application as waterborne textile finishing agent. *J. Polym. Sci. Part A Polym. Chem.* **2019**, *57*, 1305–1314. [[CrossRef](#)]
33. Zhou, J.; Li, Y.; Li, H.; Yao, H. Cellulose nanocrystals/fluorinated polyacrylate soap-free emulsion prepared via RAFT-assisted Pickering emulsion polymerization. *Colloids Surf. B.* **2019**, *177*, 321–328. [[CrossRef](#)]
34. Kedzior, S.A.; Graham, L.; Moorlag, C.; Dooley, B.M.; Cranston, E.D. Poly (methylmethacrylate)-grafted cellulose nanocrystals: One-step synthesis, nanocomposite preparation, and characterization. *Can. J. Chem. Eng.* **2016**, *94*, 811–822. [[CrossRef](#)]
35. Wei, L. All acrylic based thermoplastic elastomers: Design and synthesis for improved mechanical performance. Ph.D. Thesis, University of Tennessee, Knoxville, TN, USA, 2017.
36. Hasa, E.; Tai, Y.L.; Guymon, C.A. Controlling phase separated domains in UV-curable formulations with H-functionalized prepolymers. *Polym. Chem.* **2022**, *13*, 3102–3115. [[CrossRef](#)]
37. Michael, V.K.; Amir, S.P.; Richard, M.B.; Todd, H.; Marc, A.D.; Emily, D.C. Incorporation of polymer-grafted cellulose nanocrystals into latex-based pressure-sensitive adhesives. *ACS Mater. Au* **2022**, *2*, 176–189.
38. Yu, Q.; Yang, W.; Wang, Q.; Dong, W.; Du, M.; Ma, P. Functionalization of cellulose nanocrystals with  $\gamma$ -MPS and its effect on the adhesive behavior of acrylic pressure sensitive adhesives. *Carbohydr. Polym.* **2019**, *217*, 168–177. [[CrossRef](#)]
39. Che, K.M.; Zhang, M.Z.; He, J.L.; Ni, P.H. Polyphosphoester-modified cellulose nanocrystals for stabilizing Pickering emulsion polymerization of styrene. *Chin. J. Polym. Sci.* **2020**, *38*, 921–931. [[CrossRef](#)]
40. Xu, P.; Cao, Y.; Wu, B.; Ma, P.; Dong, W.; Bai, H.; Zhang, H.; Zhu, H.; Chen, M. Effects of modified nanocrystalline cellulose on the hydrophilicity, crystallization and mechanical behaviors of poly(3-hydroxybutyrate-co-3-hydroxyhexanoate). *New J. Chem.* **2018**, *42*, 11972–11978. [[CrossRef](#)]
41. Jie, Y.; Dai, Y.Y. Liquid crystal of nanocellulose whiskers' grafted with acrylamide. *Chin. Chem. Lett.* **2012**, *23*, 367–370.
42. Han, S.; Lyu, S.; Chen, Z.; Fu, F.; Wang, S. Combined stabilizers prepared from cellulose nanocrystals and styrene-maleic anhydride to microencapsulate phase change materials. *Carbohydr. Polym.* **2020**, *234*, 115923. [[CrossRef](#)] [[PubMed](#)]
43. Kurukji, D.; Pichot, R.; Spyropoulos, F.; Norton, I.T. Interfacial behaviour of sodium stearoyllactylate (SSL) as an oil-in-water Pickering emulsion stabiliser. *J. Colloid Interface Sci.* **2013**, *409*, 88–97. [[CrossRef](#)] [[PubMed](#)]
44. Pang, B.O.; Zhang, H.; Schilling, M.; Liu, X.; Wang, X.; Florian, R.; Zhang, K. High-internal-phase Pickering emulsions stabilized by polymeric dialdehyde cellulose-based nanoparticles. *ACS Sustain. Chem. Eng.* **2020**, *8*, 7371–7379. [[CrossRef](#)]
45. Wang, F.; Zhu, Y.; Xu, H.; Wang, A. Preparation of carboxymethyl cellulose-based macroporous adsorbent by eco-friendly Pickering-MIPs template for fast removal of  $Pb^{2+}$  and  $Cd^{2+}$ . *Front. Chem.* **2019**, *7*, 603. [[CrossRef](#)]
46. He, Y.; Wu, F. Factors that affect Pickering emulsions stabilized by graphene oxide. *ACS Appl. Mater. Interfaces* **2013**, *5*, 4843–4855. [[CrossRef](#)] [[PubMed](#)]
47. Mazela, B.; Tomkowiak, K.; Jones, D. Strength and moisture-related properties of filter paper coated with nanocellulose. *Coatings* **2022**, *12*, 1376. [[CrossRef](#)]